15th IFK
Proc. of the 15th International Fluid Power Conference <Symposium/Conference>
<DOI>

Determination of Gas Solubility for Technical and Flammable Fluids

Marius Hofmeister, Lukas Boden, Andris Rambaks, Katharina Schmitz

Institute for Fluid Power Drives and Systems, marius.hofmeister@ifas.rwth-aachen.de

Institute for Fluid Power Drives and Systems, lukas.boden@ifas.rwth-aachen.de

Institute for Fluid Power Drives and Systems, andris.rambaks@ifas.rwth-aachen.de

Institute for Fluid Power Drives and Systems, katharina.schmitz@ifas.rwth-aachen.de

Abstract

Dissolved gas is a critical factor in many technical systems, since it influences fluid properties like compressibility, viscosity or thermal conductivity in a negative manner. Cavitation due to dissolved gas can lead to damage of components and increased wear in hydraulic applications. Therefore, a precise understanding of the dissolving and release processes of gases in liquids is essential for efficient and reliable hydraulic systems.

Despite its relevance for technical applications, literature on the gas solubility of hydraulic oils and lubricants is sparse. This is particularly true for data above ambient pressure at pressures relevant for hydraulic application. To close this gap, a measurement set up using volumetric-manometric approach was designed, which can be used to determine the gas solubility of hydraulic oils and other technical liquids. For the investigation of flammable or hazardous liquid/gas combinations an indirect measurement method was developed. In this contribution the design of the measurement set up is presented as well as results for one hydraulic oil in combination with nitrogen. Based on the obtained results, it is evident that substantial amounts of gas may be released during the operation of hydraulic systems.

1. INTRODUCTION

The ability of a liquid to dissolve gas is of great importance for a variety of technical applications. For example, the formation of bubbles in hydraulic systems is influenced by the amount of dissolved gas in the fluid. Bubbles are generally undesirable in hydraulic systems as they can lead to cavitation damage and have a negative impact on fluid properties such as compressibility or viscosity. Therefore, a precise understanding of the dissolving and release processes of gases in liquids is essential for efficient and reliable hydraulic systems [1, 2].

The same applies to cooling systems where bubbles and foam hinder heat transfer between liquid and environment. This becomes increasingly important in terms of the ongoing growth of e-mobility, as efficient temperature management is a prerequisite for e-motors with high power density and battery systems with large storage capacities. Gas solubility

also plays a crucial role for combustion engines. Gaseous fuel or combustion gases can dissolve in the lubricating film on the cylinder wall and be drawn in via the piston and thus accumulate in the engine oil. This is particularly important for alternative fuels such as ammonia or hydrogen, which are either toxic or highly explosive [3].

Although gas solubility is extremely relevant for many technical applications as described, gas solubility values can only be found to a limited extent in the literature. Coefficients for gas solubility are mainly available for short-chain molecules and pure liquids. Especially, information on pressure dependent gas solubility is very sparse, since most measurements were performed at ambient pressure. Solubility data in the range of pressures relevant for hydraulic applications is primarily available for crude oil or bitumen, but not for lubricants and hydraulic oils [4].

For this reason, this article will examine the gas dissolving capacity of various hydraulic oils. To determine the gas solubility, several measurement approaches are available [5, 6]. Traditionally, these can be categorized into chemical and physical methods [5]. For analyzing gas solubility in liquids, physical methods are generally more appropriate [5]. These physical approaches can be further divided into manometric-volumetric, mass spectrometric, gas chromatographic, and radiometric techniques [5, 6]. Currently, there is no standardized procedure for determining the solubility of gases in liquids [5]. However, the literature provides some examples of experimental setups used to investigate gas solubility at elevated pressures [7, 8].

In this contribution a volumetric-manometric approach was utilized for the determination of gas solubility at different temperatures and pressures, which is based on preliminary work by Rambaks et al. [9] and has been extensively revised [3]. In the following, first the basic measuring principle is described. Then the design of the test bench and the measurement process are shown. A particular focus is on the determination of gas solubility for highly reactive or toxic liquid/gas mixtures using an indirect measurement method.

Finally, the measurement results for hydraulic oil will be presented. Where possible, the results are compared with data from the literature. Both pressure- and temperature-dependency of the Bunsen coefficient is evaluated by means of the Krichevsky Kasarnovsky equation and the Henry–Van't Hoff relationship. With help of the corresponding parameters the interpolation and extrapolation of the measured data is possible.

2. METHODOLOGY

In the literature, various definitions and measures are used to describe the ability of liquids to dissolve gases. Therefore, this work first provides a general overview of the relevant variables and definitions employed herein, followed by a description of the measurement procedure and its fundamental functionality. Then, the thermodynamic principles underlying the method are derived, and the applicability of the approach to hazardous or flammable gas–liquid systems is discussed.

2.1. Definition of gas solubility

The most common measures used to represent gas solubility are listed in Table 2.1. The most fundamental quantity is the concentration c_G, which expresses the amount of dissolved gas n_G per unit volume of liquid V_L, typically in $\mathrm{mol/m^3}$. Alternatively, the mole fraction x_G

represents the ratio of dissolved gas moles n_G to the total moles of all components in the liquid phase ($n_G + n_L$). This dimensionless quantity is widely employed in thermodynamic modeling. Henry's law constant k_H establishes a proportional relationship between the equilibrium gas partial pressure p and its concentration c_G in the liquid. It serves as a convenient measure to relate experimentally accessible pressures to dissolved amounts, particularly in dilute solutions where the law holds. The Bunsen coefficient is defined as the volume of gas V_G (referred to standard conditions, e.g. $T_0 = 298.15$ Kand $p_0 = 1$ bar) that dissolves in a unit volume of liquid V_L under a partial pressure p.

Table 2.1 Summary of definitions and interrelations of gas solubility parameters

	Concentration $[\mathrm{mol \cdot m^{-3}}]$	Mole fraction [–]	Henry constant $[\mathrm{Pa \cdot m^3 \cdot mol^{-1}}]$	Bunsen coefficient [–]
	$c_G = \frac{n_G}{V_L}$	$x_G = \frac{n_G}{n_G + n_L}$	$k_H = \frac{p}{c_G}$	$\alpha = \frac{V_G}{V_L}\frac{p_0}{p}$
$f(c_G)$	—	$x_G = c_G \frac{M_L}{\rho_L}$	$k_H = \frac{p}{c_G}$	$\alpha = c_G \frac{RT_0}{p_0}$
$f(x_G)$	$c_G = x_G \frac{\rho_L}{M_L}$	—	$k_H = \frac{M_L p}{\rho_L}\frac{x_G}{1 - x_G}$	$\alpha = x_G \frac{RT_0}{p_0}\frac{\rho_L}{M_L}$
$f(k_H)$	$c_G = \frac{p}{k_H}$	$x_G = \frac{pM_L}{k_H \rho_L + pM_L}$	—	$\alpha = \frac{1}{k_H}\frac{RT_0 p}{p_0}$
$f(\alpha)$	$c_G = \alpha \frac{p_0}{RT_0}$	$x_G = \alpha \frac{p_0}{RT_0}\frac{M_L}{\rho_L}$	$k_H = \frac{1}{\alpha}\frac{RT_0 p}{p_0}$	—

Since the Bunsen coefficient has historically been used to describe the gas solubility of hydraulic oils and many other technical liquids, this parameter will also be used in this paper. In addition, many oils are mixtures with largely unknown compositions, meaning that no molar mass M_L can be determined and the amount of substance n_L cannot be calculated for a given liquid volume V_L either. As shown in Table 2.1, the parameters used to describe the ability of liquids to dissolve gases can be converted into one another if necessary.

2.2. General determination of gas solubility according to the manometric-volumetric principle

In this study, the Bunsen coefficient is determined by using a volumetric-manometric method, in which different states of a defined gas volume in thermodynamic equilibrium are evaluated. The pressure in the gas phase is used to quantify the amount of gas that has dissolved in the liquid as illustrated in **Figure 2.1**. The gas and liquid phases are at the same temperature and pressure. In the initial state (0), the liquid contains no dissolved gas, whereas in state 1, a certain amount of gas has already dissolved in the liquid.

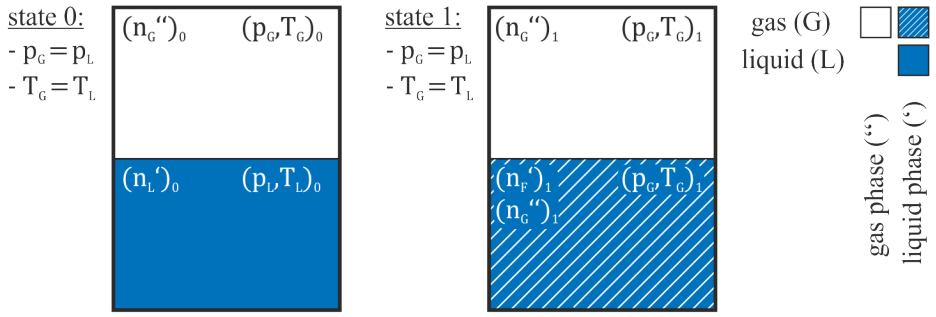

Figure 2.1. Ideal closed system

Since the example system is a closed system, the total amount of gas $(n_G)_i$ is constant and can be represented as the sum of the amount of dissolved gas $(n_G')_i$ and free gas in the gaseous phase $(n_G'')_i$ (2.1).

$$(n_G)_i = (n_G')_i + (n_G'')_i = \text{const.} \tag{2.1}$$

The amount of gas $(n_G'')_i$in the gaseous phase can be described using the real gas law, which is a function of temperature $(T_G'')_i$ and pressure $(p_G'')_i$ as well as the gas volume $(V_G'')_i$, the gas constant R and the compressibility factor $(z_G)_i$.

$$(n_G'')_i = \frac{1}{R}\left(\frac{p_G'' V_G''}{T_G'' z_G}\right)_i \tag{2.2}$$

The amount of dissolved gas $(n_G')_1$ in state 1 corresponds to the difference of the amount of gas in the gaseous phase in state 0 $(n_G'')_0$ and state 1 $(n_G'')_1$. The underlying assumption is that the amount of dissolved gas in state 0 $(n_G'')_0$ is equal to 0.

$$(n_G')_1 - \underbrace{(n_G')_0}_{\approx 0} = (n_G'')_0 - (n_G'')_1 \tag{2.3}$$

As shown in Table 2.1 Bunsen coefficient α_i is the ratio of dissolved gas volume at standard conditions $(V_G')_S$ and the liquid volume $(V_L')_S$. In accordance with the ideal gas law, the gas volume can be also expressed as a function of $(n_G')_S$.

$$\alpha_i = \frac{(V_G')_S}{(V_L')_S} = \frac{R(T)_S}{(V_L')_S (p'')_S}(n_G')_S \tag{2.4}$$

By combining equations (2.2), (2.3) and (2.4), the resulting expression (2.5) is obtained. Finally, the Bunsen absorption coefficient can be determined by comparing the state variables temperature and pressure in both states and by evaluating the volumes $(V_L')_i$ and $(V_G'')_i$.

$$\alpha_i = \frac{(T)_S}{(V_L')_S (p'')_S}\left[\left(\frac{p'' V_G''}{T''}\right)_0 - \left(\frac{p'' V_G''}{T''}\right)_1\right] \tag{2.5}$$

2.3. Measurement setup

For practical implementation of the measurement method described above and to determine the unknown parameters from equation (2.5), the test bench shown in **Figure 2.2** was used. The setup mainly consists of a cylinder which can be filled with liquid and gas. To determine the state variables p'' and T'', corresponding pressure and temperature sensors are located inside the cylinder. The pressure in the gas and liquid phase is equal, so that a single sensor is sufficient to obtain the required pressure data. Since gases and liquids generally heat up at different rates when pressure changes, two separate temperature sensors are used for the respective phases. The volume of the gas phase $(V_G'')_i$ can be calculated using equation (2.6). The piston position x required for this is measured by the installed LVDT sensor.

$$(V_G'')_i = (V_L')_i - [V_0 + A(x_0 - x)] \tag{2.6}$$

The initial volume of the cylinder V_0 was determined in advance by filling it with water. To do this, a container was filled with water and weighed with a precision scale both before and after pouring it into the cylinder. The accuracy of the scale is 0.01 g. The total volume of the cylinder V_0 can then be calculated in accordance with equation (2.7).

$$V_0 = \frac{(m'_{H2O})_0}{(\rho'_{H2O})_0}, \qquad (V_L')_0 = \frac{(m'_L)_0}{(\rho'_L)_0} \tag{2.7}$$

Before filling the test liquid, its mass is also weighed using a precision scale, so that the same relationship as in equation (2.7) can be applied to determine $(V_L')_i$. The required density values are either taken from the literature or determined according to standard DIN 12790 [10]. Changes of $(V_L')_i$ due to compression are neglectable for most liquids at low pressures and are considered for high pressures using a suitable density model.

Adjusting the piston changes the cylinder volume and, thus, the thermodynamic state of the system, enabling the comparison of different states according to equation (2.5).

After the filling process, the cylinder is sealed. To avoid contamination from dissolved gases and the ambient air above the liquid, the cylinder is connected to a vacuum pump. The pump allows the gas phase inside the cylinder to be evacuated, while the resulting pressure reduction promotes the release of any gases previously dissolved in the liquid. During evacuation, care must be taken to ensure that the pressure does not fall below the vapor pressure of the liquid.

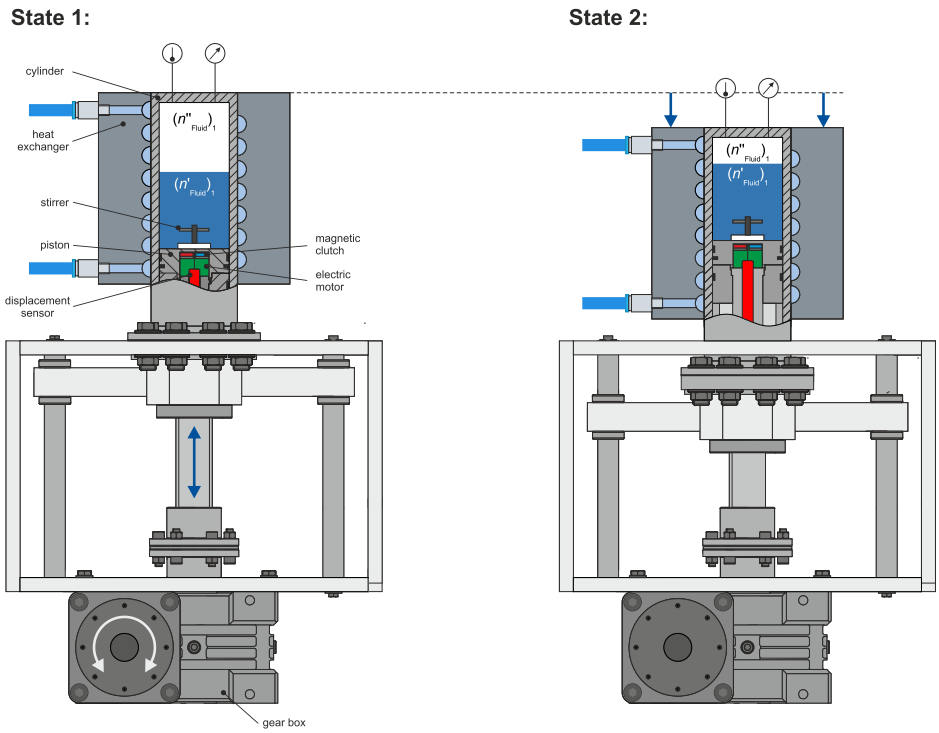

Figure 2.2. Bunsen test bench

After the evacuation of the cylinder, the chamber pressure and volume are adjusted using the piston position. A control loop is implemented to regulate the deviation between the setpoint and the actual pressure in the cylinder, which is translated into a motion of the stepper motor. The stepper motor is mechanically coupled to the piston via a gearbox. In the exemplary measurement shown in **Figure 2.3**, a chamber pressure of 18 bar was set for the first measuring point (1), corresponding to a piston position of approximately 38.8 mm. The increased pressure drives the system out of thermodynamic equilibrium, causing gas to start dissolving into the test liquid. To accelerate the diffusion process, the stirrer mounted on the piston is activated indicated by voltage U. If no change in pressure and temperature outside a small tolerance range can be detected, it is assumed that thermodynamic equilibrium has been reached again. To ensure that the measurement is not influenced by heat generated by the stirrer, it is turned off prior to data acquisition (voltage U: 2 V → 0 V). Thereafter, the quantities temperature T, pressure p, and piston displacement x are recorded for a duration of 10 minutes.

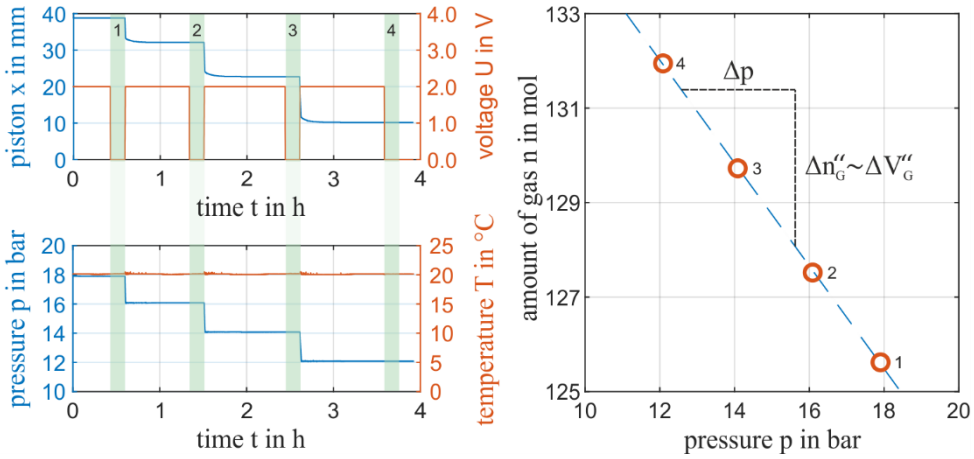

Figure 2.3. Example measurement trace showing the recorded signals

This procedure was repeated for three additional measurement points at 16, 14, and 12 bar. Using the mean values of the recorded quantities, a regression analysis based on equation (2.5) can be performed, as illustrated in the right panel in Figure 1. The slope of the resulting dashed line corresponds to the Bunsen coefficient at the given temperature of 20 °C.

To maintain a constant temperature level, a heat exchanger is mounted on the cylinder. The heat exchanger is connected to a tempering unit controlled by the measuring computer. With help of the temperature signals a closed control loop is feasible. The utilized material for the heat exchanger allows operating temperatures between -20 and +80 °C. In combination with the stepper motor, the described temperature control allows the automated measurement of pressure/temperature maps up to 400 bar. The lower pressure limit is primarily constrained by the vapour pressure of the investigated liquid; in principle, pressures below ambient conditions are attainable.

2.4. Indirect determination of gas solubility for flammable and hazardeous liquid/fuel combinations

The handling of certain mixtures of technical fluids and gases involves significant safety risks. Fuels, as well as hydraulic oils and other lubricants, can ignite upon contact with oxygen. In the context of carbon-free combustion, gaseous fuels such as hydrogen and ammonia, which can be dissolved in considerable amounts in the engine oil of internal combustion engines, are becoming increasingly relevant. In the case of hydrogen, there is a high risk of explosion due to its strong reactivity, whereas ammonia poses serious environmental and health hazards at elevated concentrations. To determine the Bunsen coefficient of such mixtures safely, an indirect measurement method was developed. [3]

Whether a potentially explosive mixture ignites depends on the composition of the gaseous phase. This relationship is illustrated in **Figure 2.4** for a hypothetical ternary system. The a-axis represents the volumetric fraction of vaporized oil or fuel in the gas phase, while the b- and c-axes indicate the respective fractions of nitrogen and oxygen. Mixtures located within the yellow explosion region can potentially ignite.

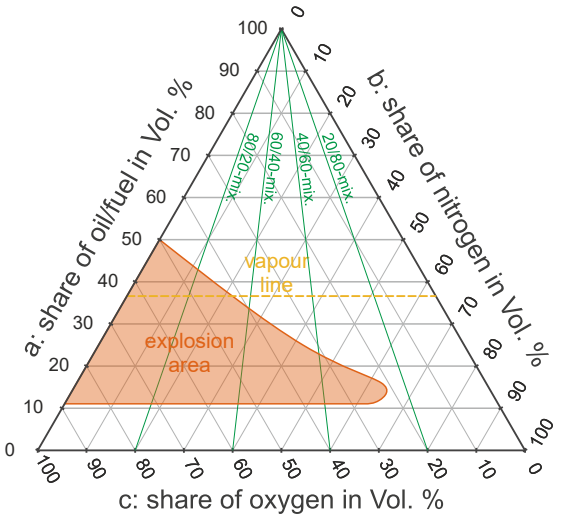

Figure 2.4. flammability diagram for hypothetical oil(fuel)/gas mixture

To estimate the explosion risk of a specific oil or fuel, the molar fraction x_i of the vaporized liquid in the gas phase is calculated according to Raoult's and Henry's law. According to equation (2.8), the molar fraction can be expressed as a function of the total pressure p and the vapor pressure p_i of the liquid.

$$p_{vap} = p \cdot x_i \iff x_{vap} = \frac{p_{vap}}{p} \tag{2.8}$$

Assuming an ideal gas behavior, the molar fraction x_i is equal to the volumetric fraction, and the vapor line (orange) can be plotted in Figure 2.4. For low pressures the volumetric fraction of the vapor increases, while at higher pressures it decreases.

The ratio of the remaining gases, oxygen and nitrogen, is indicated by the green lines in Figure 2.4 and corresponds to the original composition of the gas phase during the filling of the test bench. For an N_2/O_2 ratio of 20/80, the intersection with the vapor line falls within the explosion region. Increasing the fraction of nitrogen shifts the intersection to the right, so that, for example, for synthetic air (N_2/O_2 = 80/20) it lies outside the explosion region. By adjusting the composition of the gas phase in the cylinder, the risk of explosion can thus be eliminated. Similarly, this approach can be used to reduce the toxicity of hazardous gases such as ammonia by mixing them with inert gases.

With the presence of a gas mixture, the Bunsen coefficient of the individual pure components can no longer be determined directly using the method described in Section 2.3. Instead, the Bunsen coefficient of the mixture α_{mix} can be evaluated, based on the individual Bunsen coefficients of the constituent gases and their respective molar fractions (2.9).

$$\alpha_{mix} = \alpha_{N2} \cdot x_{N2} + \alpha_{O2} \cdot x_{O2} \iff \alpha_{O2} = \frac{\alpha_{mix} - \alpha_{N2} \cdot x_{N2}}{x_{O2}} \tag{2.9}$$

By rearranging (2.9), the Bunsen coefficient of oxygen α_{O2} can be determined for the example illustrated in Figure 2.4, based on the corresponding values of the mixture and of pure nitrogen ($\alpha_{mix}, \alpha_{O2}$).

3. RESULTS AND DISCUSSION

Measurements were carried out for hydraulic oil. The results for the temperature and pressure dependent Bunsen coefficient of a HLP 46 oil and nitrogen are shown in **Figure 3.1** [11]. The Bunsen coefficient was determined for pressures between 150 and 350 bar and temperatures ranging from 273.15 K to 323.15 K. The pressure was varied in 50 bar increments and the temperature in increments of 25 K. For each temperature and pressure step two measurements were conducted. The shown results correspond to the mean value obtained for all sensor signals recorded over a duration on 10 minutes with a frequency of 1 Hz. The left panel shows the Bunsen coefficient as a function of pressure, while the right panel illustrates the effect of temperature on gas solubility. The dashed lines indicate model data obtained from a regression analysis. The underlying equations of the analysis will be described later. The measured values for an identical measuring point in some cases differ greatly from one another. This deviation is particularly large for high pressures and low temperatures. Here, the measured Bunsen coefficient for identical boundary conditions differs by a value of 0.005.

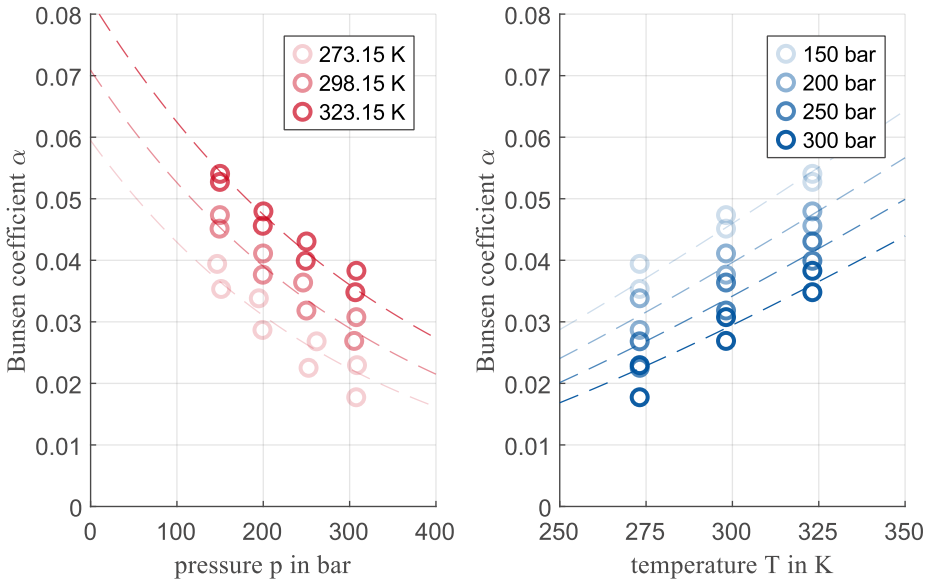

Figure 3.1. Bunsen coefficient of HLP 46 and nitrogen

As can be seen, the Bunsen coefficient decreases for rising pressure values. This trend is consistent with the behavior that emerges from the Krichevsky-Kasarnovsky equation (3.1) for positive values of the partial molar volume ΔV_{solv}. [12]

$$\alpha(p,T) = \alpha(p_0,T) \cdot \exp\left[-\frac{\Delta V_{solv}}{RT}(p - p_S)\right] \tag{3.1}$$

The dependence of gas solubility on temperature can be described using the Henry–Van't Hoff relationship in equation (3.2). According to this, gas solubility follows an exponential curve. For a positive solution enthalpy ΔH_{solv}, increasing solubility is to be expected at rising temperatures, which is also reflected in the experiment. [13]

$$\alpha(p_0, T) = \alpha(p_0, T_0) \cdot \exp\left[\frac{\Delta H_{solv}}{R}\left(\frac{1}{T_S} - \frac{1}{T}\right)\right] \tag{3.2}$$

The nearly proportional relationship between gas solubility and temperature can be explained by the small temperature changes, where the exponential relationship from equation (3.2) can be simplified by a Taylor series expansion and approximately corresponds to the linear expression from (3.3).

$$\alpha(p_0, T) \approx \alpha(p_0, T_0) \cdot \left[1 - \frac{\Delta H_{solv}}{R{T_S}^2}(T - T_S)\right] \tag{3.3}$$

Based on the Krichevsky-Kasarnovsky equation and the Henry–Van't Hoff relationship a regression analysis was performed using a trust-region-reflective algorithm to minimize the sum of squared residuals while accounting for parameter bounds. The derived values for ΔV_{solv}, ΔH_{solv} and $\alpha(p_0, T_0)$ are listed in **Table 3.1** together with the corresponding goodness-of-fit criteria ($R^2, {R^2}_{adj.}, SSE$). Here, the coefficient of determination R^2 quantifies the proportion of variance in the dependent variable that is explained by the model. The adjusted coefficient of determination ${R^2}_{adj.}$ accounts for the number of model parameters and penalizes overfitting. The sum of squared errors (SSE) represents the cumulative squared deviation between observed and predicted values and serves as an absolute measure of the model's residual error. Even though the values for identical measurement points in some cases diverge significantly, the high values for R^2 and ${R^2}_{adj.}$ and low values for SSE indicate that the measurement method is capable of representing the underlying physical laws that determine the pressure- and temperature-dependent gas solubility of oils.

Thermodynamic measures		Goodness-of-fit criteria	
$\alpha(p_0, T_0)$	0.0709	R^2	0.952
ΔV_{solv}	$7.3955\ \frac{m^3}{mol}$	${R^2}_{adj.}$	0.947
ΔH_{solv}	$4756.1\ \frac{J}{mol}$	SSE	$1.015e-4$

Table 3.1 Thermodynamic measures and goodness-of-fit criteria for HLP 46

Since the recorded measurement signals− and consequently the calculated Bunsen coefficient−showed only minor deviations for a single measuring point, the corresponding error bars are not visible in Figure 3.1. Therefore, a detailed analysis of the recorded sensor signals was conducted, as shown in **Figure 3.2**.

The results are shown in Figure 3.2 in the form of box plots, illustrating the deviations from the respective mean value of each measurement. It can be observed that, for the pressure, both the lower and upper quartiles lie within a band of at least ±0.5 bar, indicating a low

pressure variability. Furthermore, the median is located close to the mean value, suggesting a symmetric and evenly distributed temperature signal. The observed deviations can be primarily attributed to uniform noise in the measurement signal, with external influences exerting negligible impact.

For the temperature measurements, the boxes indicate greater variability in both magnitude and position relative to the mean. Nevertheless, the overall deviations are minor, with both the lower and upper quartiles confined to a range of approximately ±0.05 °C.

Deviations in piston position are also minimal, on the order of a few hundredths of a millimeter. Notably, the median consistently lies above the mean value across all measurements, suggesting the presence of a systematic error. Additionally, two individual data points exhibit larger deviations.

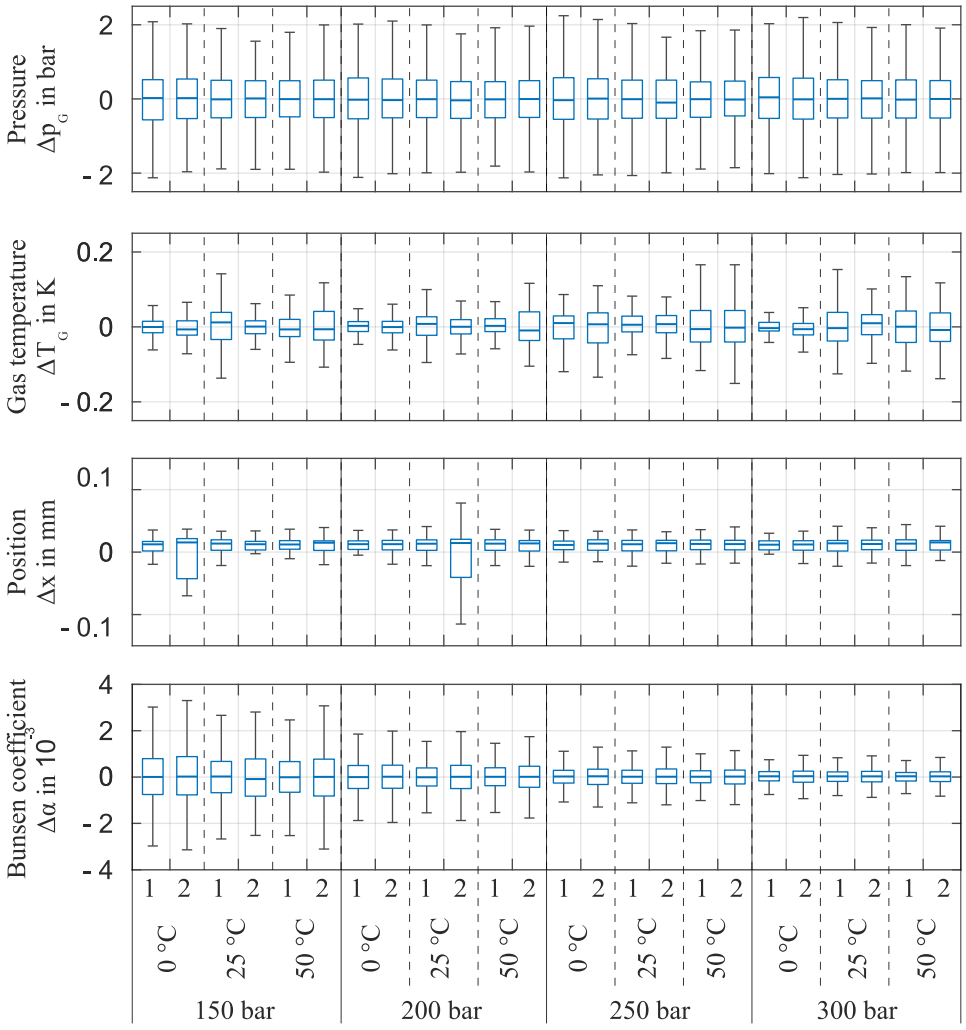

Figure 3.2. Statistical deviations of the sensor signals (gas temperature T_G, pressure p_G, and position x) and the resulting deviations of the Bunsen coefficient α.

Despite the asymmetries observed in the temperature and position data, the Bunsen coefficient demonstrates a uniform distribution around the mean. The bounds of the upper and lower quartiles remain within a narrow range of ±0.001. It is, however, evident that the coefficient values at lower pressures exhibit greater scatter compared to those at higher pressures, whereas temperature appears to have no significant influence on the variation. Consequently, the discrepancies between the two measurement series from Figure 3.1 are unlikely to result from measurement errors. A more plausible explanation is that improper filling of the test rig led to inaccurate assumptions regarding the volumes of liquid and gas and therefore to small deviations between both measurement series.

Since the composition of hydraulic oils is widely unknown, validation with literature data is difficult. The exact composition of the investigated oil is also unknown, so that no calculation of the Bunsen coefficient based on data for pure liquids is possible. However, it can be assumed that HLP oils consist of a mixture of paraffins, naphthenes, and aromatics, allowing for a comprehensive plausibility check [14]. Gas solubility data for the named molecule groups were transferred to the Bunsen coefficient using the interrelations from Table 2.1 and assembled in Figure 3.3 [15]. As can be seen, for most listed hydrocarbons the ability to dissolve nitrogen decreases increasing number of C-atoms. The Bunsen coefficient of the investigated HLP oil is lower than for all n-Alkanes with number of C-atoms lower than 20 and all other hydrocarbons listed. Given that mineral oil-based hydraulic oils within this viscosity class can contain hydrocarbons ranging between 15 and 50 C-atoms, the measured value of 0.0709 seems plausible [16].

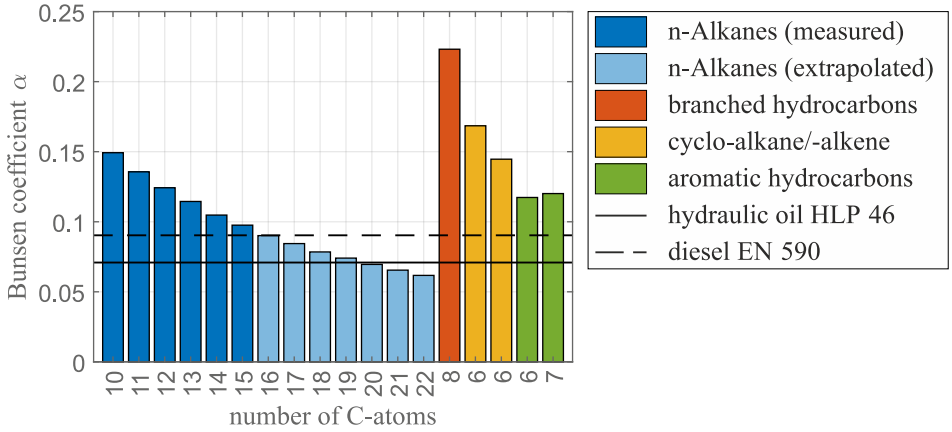

Figure 3.3. Comparison of literature data for the Bunsen coefficient of different hydrocarbons and nitrogen [15]

In a previous study, diesel EN 590 was examined and a Bunsen coefficient of 0.903 was determined [17]. Given that the gas solubility of the hydrocarbons considered decreases with increasing number of C-atoms, the lower values for the comparatively long-chain HLP 46 (Diesel: C13 - C18) are plausible, too [18].

Of particular interest for hydraulic systems is the amount of gas that can be released during operation, as cavitation may damage components and the fluid mechanical properties of the oil can be affected by undissolved gas.

Using the parameters from Table 3.1 and Equations 3.1–3.2, the volume of dissolved gas at standard conditions per unit volume of oil was calculated for pressures and temperatures typical of hydraulic applications. **Figure 3.4** shows that, at high pressures and temperatures, theoretically large amounts of nitrogen can dissolve. For instance, at 400 bar and 80 °C, the gas volume reaches nearly 14 times the oil volume. However, under such extreme conditions, achieving equilibrium is highly unlikely because dissolution processes are slow and gas may immediately re-release at ambient pressure in the tank.

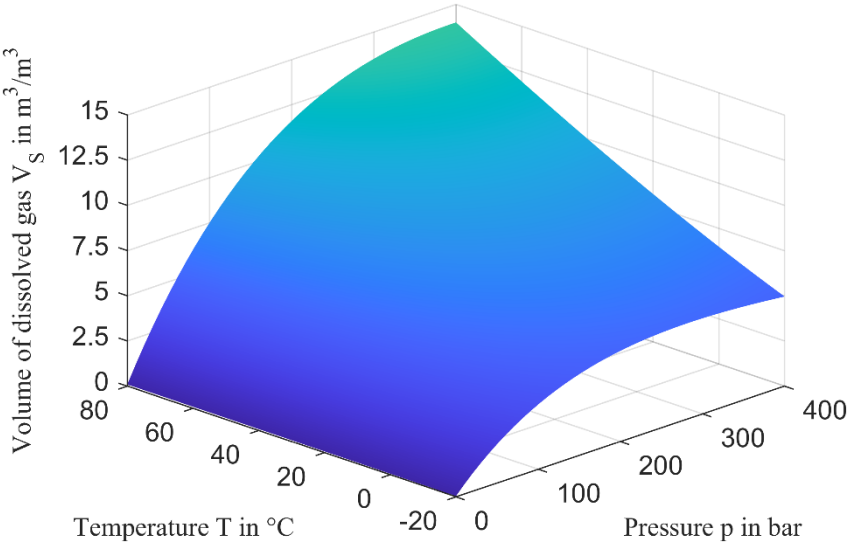

Figure 3.4. Volume of dissolved nitrogen at standard conditions per unit volume of oil

For practical hydraulic operation, the amount of gas that can dissolve under tank pressure and temperature is more relevant. Assuming a system operating at 40 °C and tank pressure equal to ambient, approximately 7.77 % of the oil volume could be saturated with gas. If the pressure drops by 0.1 bar, as might occur in a suction line, the dissolved gas fraction would decrease to 6.99 %, corresponding to about 0.78 % of the oil volume forming bubbles.

Gas release can also be triggered by temperature changes. For example, consider a mobile hydraulic machine operating with a tank temperature of 50 °C. During operation, the oil has sufficient time to reach saturation under these conditions. If the machine is then stored outdoors at −20 °C, and assuming released bubbles remain trapped within pipes, cylinders, or pump housings, the gas volume would occupy approximately 3.18 % of the oil volume after cooling to ambient temperature.

These examples demonstrate that, under normal operating conditions, only a small fraction of the maximum solubility of hydraulic oils is realized. Nevertheless, both operational and standstill conditions can lead to the release of relative gas volumes of a few percent of the oil volume, which may still be significant for system performance. It should be noted that these estimations are based solely on nitrogen values. Accurate determination would require the Bunsen coefficient for oxygen; however, since air consists predominantly of nitrogen, the results are considered to be of the correct order of magnitude.

4. SUMMARY AND OUTLOOK

In this study, a measurement principle for determining the gas solubility of technical liquids was presented, and pressure- and temperature-dependent results for a hydraulic oil (HLP 46) were discussed. Although a direct validation of the results using literature data is challenging, the obtained values were found to be plausible and in good agreement with the underlying thermodynamic models. The obtained gas solubility values indicate that, during hydraulic system operation, dissolved gas can occupy a few percent of the oil volume, potentially causing cavitation and altering the fluid properties of the oil.

In future work, additional oils will be investigated to analyze the influence of oil composition and additives on gas solubility in more detail. Of particular relevance is the study of the solubility behavior of alternative gaseous fuels such as hydrogen and ammonia in engine oils. Understanding how much of these gases can be dissolved, how much may be released to the environment, and how the dissolved gases affect oil degradation is essential for safe and efficient engine operation. Within the framework of the Excellence Cluster *The Fuel Science Center*, a simulation model is currently being developed to describe gas diffusion within the lubricating film between piston ring and cylinder wall. The required material data will be determined experimentally using the measurement method presented in this work.

5. NOMENCLATURE

α	Bunsen coefficient	$[-]$	R^2_{adj}	coefficient of determination (adjusted)	$[-]$
ρ	density	$\left[\frac{kg}{m^3}\right]$	SSE	sum of square due to error	$[-]$
A	piston surface	$[\,m^2\,]$	T	temperature	$[\,K\,]$
c	concentration	$\left[\frac{mol}{m^3}\right]$	SSE	sum of square due to error	$[-]$
ΔH	enthalpy	$[\,J\,]$	t	time	
k_H	Henry's law constant	$\left[\frac{Pa \cdot m^3}{mol}\right]$	U	voltage	
m	mass	$[\,kg\,]$	V	volume	
M	molar mass	$\left[\frac{kg}{mol}\right]$	ΔV_{solv}	partial molar volume	
n	amount of substance	$[\,mol\,]$	x_i	mole fraction	
p	pressure	$[\,bar\,]$	z	compressibility factor	
R^2	coefficient of determination	$[-]$			

$(\dots)_G$	gas	$(\dots)_1$	state 1
$(\dots)_L$	liquid	$(\dots)'$	liquid phase
$(\dots)_S$	standard conditions	$(\dots)''$	gas phase
$(\dots)_0$	initial state		

6. ACKNOWLEDGEMENTS

This work was funded by the German Research Foundation (DFG) in the scope of the project „Einfluss der Belastungsgradienten auf das Ermüdungsverhalten hydraulischer Komponenten" with the number 449676223, and under Germany´s Excellence Strategy – Exzellenzcluster 2186 „The Fuel Science Center".The authors would like to thank DFG for its support.

7. REFERENCES

[1] YOUNG, F. Ronald: *Cavitation*. London : Imperial College Press, 1999

[2] NIKOLAJSEN, Jorgen L.: *Viscosity and Density Models for Aerated Oil in Fluid-Film Bearings©*. In: *Tribology Transactions* 42 (1999), Nr. 1, S. 186–191. 10.1080/10402009908982207

[3] MARIUS HOFMEISTER, et al.: Solubility of Ammonia and Hydrogen in Engine Oils. 10.13140/RG.2.2.13368.05127. In: FSC (Hrsg.): *13th International Conference : Fuel Science - From Production to Propulsion, 2025*, 2025

[4] V. P. LOGVINYUK, V. V. MAKARENKOV, V. V. MALYSHEV & G. M. PANCHENKOV: *Solubility of gases in petroleum products*. In: *Chemistry and Technology of Fuels and Oils* (1970), Volume 6, pages 353–355

[5] BATTINO, Rubin, et al.: *The Solubility of Gases in Liquids*. In: *Chemical Reviews* 66 (1966), Nr. 4, S. 395–463. 10.1021/cr60242a003

[6] *The experimental determination of solubilities*. Chichester : Wiley, 2003 (Wiley series in solution chemistry 6)

[7] HUANG, Sam S.-S., et al.: *The phase behavior of two mixtures of methane, carbon dioxide, hydrogen sulfide, and water*. In: *Fluid Phase Equilibria* 19 (1985), 1-2, S. 21–32. 10.1016/0378-3812(85)85033-0

[8] ROUSSEAUX, P., et al.: *A static method for determination of vapour—liquid equilibria and saturated liquid molar volumes at high pressures and temperatures using a new variable-volume cell*. In: *Fluid Phase Equilibria* 11 (1983), Nr. 2, S. 153–168. 10.1016/0378-3812(83)80055-7

[9] RAMBAKS, Andris, et al.: METHOD FOR THE EXPERIMENTAL DETERMINATION OF THE BUNSEN ABSORPTION COEFFICIENT OF HYDRAULIC FLUIDS, FPMC2019. 10.1093/nar/gkn369. In: *Proceedings of the ASME/BATH 2019 Symposium on Fluid Power and Motion Control*, 2019

[10] DIN 12790:2019-12. Dezember 2019. *DIN 12790: Laboratory glassware; hydrometers -Principles of construction and adjustment*

[11] FUCHS LUBRICANTS: *Safety Data Sheet Renolin B 15 VG 46*. 2017

[12] LÜDECKE, Christa, et al.: *Thermodynamik* : *Physikalisch-chemische Grundlagen der thermischen Verfahrenstechnik*. Softcover reprint of the hardcover 1st edition 2000. Berlin, Heidelberg : Springer, 2000 (Springer-Lehrbuch)

[13] CARRERO, J. I.: *Application of the van't Hoff equation to phase equilibria*. In: *ChemTexts* 10 (2024), Nr. 3. 10.1007/s40828-024-00188-x

[14] THEO MANG, et al.: *Lubricants and lubrication*. Third, completely revised and enlarged edition. Weinheim : Wiley-VCH, 2017

[15] BATTINO, Rubin, et al.: *The Solubility of Nitrogen and Air in Liquids*. In: *Journal of Physical and Chemical Reference Data* 13 (1984), Nr. 2, S. 563–600. 10.1063/1.555713

[16] EMMANUEL O. ALUYOR AND MUDIAKEOGHENE ORI-JESU: *Biodegradation of mineral oils – A review*. In: *African Journal of Biotechnology* Vol. 8 (2009), Nr. 6, 915-920

[17] HOFMEISTER, Marius, et al.: A Method for Determining the Bunsen Coefficient of Bio-Hybrid Fuels. 10.4271/2021-01-1187. In: *SAE Technical Paper Series* : SAE International400 Commonwealth Drive, Warrendale, PA, United States, 2021 (SAE Technical Paper Series).

[18] *Fuels and lubricants handbook* : *Technology, properties, performance, and testing*. 2nd edition. West Conshohocken, PA : ASTM International, 2019 (ASTM's manual 37)

Biographies

Marius Hofmeister received his master's degree in mechanical engineering from RWTH Aachen University in 2019. He is currently a research associate at the Institute for Fluid Power Drives and Systems (ifas) and a member of the Fuel Science Center, where his research focuses on alternative fuels, particularly their fluid mechanical properties and material compatibility.

Lukas Boden obtained his master's degree in mechanical engineering at RWTH Aachen University in 2023. Since then, he is working as a research associate at the Institute for Fluid Power Drives and Systems (ifas), focussing on identifying the influence of viscous fluid on fatigue crack propagation in fluid power components.

Andris Rambaks studied mechanical engineering at Riga Technical University from 2011 to 2014 and obtained his master's degree in mechanical engineering from RWTH Aachen University in 2018. From 2018 to 2023, he worked as a research associate at the Institute for Fluid Power Drives and Systems (ifas), where he focused on investigating gas solubility in hydraulic oils and the fatigue behavior of autofrettaged components.

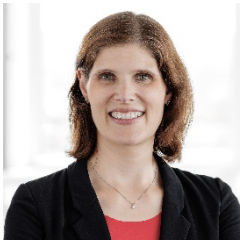

Univ.-Prof. Dr.-Ing. Katharina Schmitz studied mechanical and chemical engineering at RWTH Aachen University and Carnegie Mellon University, Pittsburgh (USA) and graduated 2015 as Dr.-Ing. at RWTH Aachen University. Since 2018, she is full professor at RWTH Aachen University and director of the Institute for Fluid Power Drives and Systems (ifas). In addition, she is Vice Dean of the Faculty for Mechanical Engineering at RWTH Aachen, a position she holds since 2020. Prof. Schmitz's awards and honors include several best paper awards and 2023 IMechE Joseph Bramah Medal award.